SHORELINE VARIATION OF AN ISLAND IN RESPONSE TO CHANGE IN WAVE DIRECTION

Takaaki Uda[1], Yasuhito Noshi[2], Takuya Yokota[3] and Masato Sekine [2]

We selected Komaka Island located 3 km offshore of Chinen Peninsula in Okinawa and surrounded by coral reef as a study site, and we conducted field observation of the shoreline changes on this coral cay on 13 July 2019, and the shoreline changes were investigated using satellite images. The shape of the sandbar behind the island was classified into one of three types (circular, slender oval, and elongated oval). Then, the changes in the sandbar were numerically simulated using the modified BG model (a model for predicting 3-D beach changes based on Bagnold's concept). In this model, waves were assumed to be incident from every direction so as to focus at the center of the circular island. Under this condition, the distribution of the wave diffraction coefficient K_d was assumed, taking the wave-sheltering effect of the cay into account, and longshore sand transport was assumed to be induced owing to the change in K_d in the direction normal to the wave direction. The results of numerical simulation explained well the deformation of the sandbar on Komaka Island.

Keywords: coral cay; Komaka Island; BG model; beach changes; numerical simulation

INTRODUCTION

On a coast surrounded by a shallow reef, a coral cay may be formed by the deposition of coral debris and foraminifera remains by waves, and shoreline variation in response to changes in wave direction can often be observed. For example, on Embudu Village Island in the Maldives, seasonal variation of a sandy beach of a coral cay was observed; the sandbar (sand spit) shape varied in response to the variation in wave direction during monsoons (Uda et al., 2017). In this case, the cay itself has a wave-sheltering effect, so the wave field around the cay changes owing to the existence of the cay, affecting the shoreline changes. Since a coral cay has a closed system in sand transport, marked shoreline changes may occur, affecting the recreational use of the island. Such topographic changes are mainly triggered by longshore sand transport owing to oblique incidence of waves to the island.

Regarding the prediction of shoreline changes of a cay, Miyahara et al. (2013) numerically simulated the deformation of a circular island composed of sand using the BG model (a model for predicting 3-D beach changes based on Bagnold's concept) (Uda et al., 2018). They employed the longshore sand transport formula with Ozasa and Brampton's term (1980) as the fundamental equation in which the additional effect due to the longshore inclination in breaker height is included, and the wave field around the island was calculated using the energy balance equation for irregular waves. In their calculation, the wave field changed in response to topographic changes, so it was recalculated every 10 steps. Serizawa et al. (2014) also predicted the interactions among multiple circular islands induced by the wave-sheltering effect of an island itself on a shallow flat seabed. In these studies, the calculation load was significantly large because of the repetition of calculation. Here, the BG model was modified, in which longshore sand transport is assumed to occur in response to the longshore inclination in wave height caused by the wave-sheltering effect of the island itself. In this study, instead of the method in which the wave field is directly calculated as in the method of Serizawa et al. (2014), a new method was developed in analogy with Ozasa and Brampton's theory (1980), in which longshore sand transport is induced by the longshore inclination in breaker height, given the distribution of K_d. We assume that waves are radially incident to the center of the circular island at any point, and that the wave height distribution changes owing to the wave-sheltering effect of the island itself. With this model, beach changes around a cay can be predicted without repeated calculation of the wave field.

GENERAL CONDITION OF STUDY SITE AND METHOD OF STUDY

The study area is Komaka Island, located approximately 3 km southwest of Chinen Peninsula in Najo City in Okinawa, Japan, and it is a coral cay formed on the shallow coral reef extending along the south boundary of Nakagusuku Bay, as shown in Fig. 1. Figure 2 shows an enlargement of the rectangular area shown in Fig. 1, including Komaka Island. This cay is located on a coral reef extending in the ENE direction from the south end of the Chinen Peninsula to Kudaka Island. Because

[1] Public Works Research Center, uda@pwrc.or.jp, 1-6-4 Taito, Taito-ku, Tokyo 110-0016, Japan
[2] Nihon University, noshi.yasuhito@nihon-u.ac.jp, 7-24-1 Narashinodai, Funabashi, Chiba 274-8501, Japan
[3] Coastal Engineering Laboratory Co., Ltd., ctr.ty.725@gmail.com, 1-22-301 Wakaba, Shinjuku-ku, Tokyo 160-0011, Japan

Figure 1. Location of Komaka Island offshore of Chinen Peninsula in Okinawa.

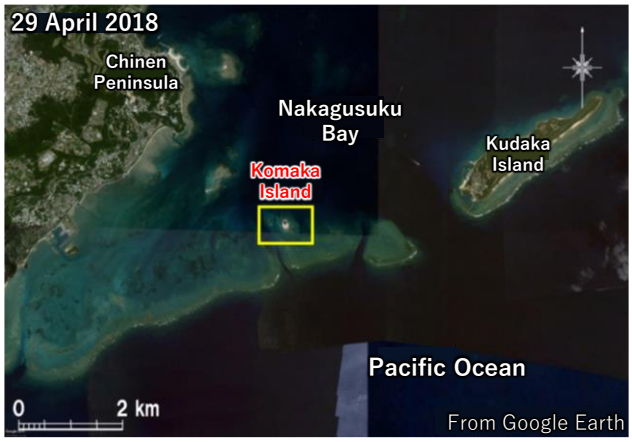

Figure 2. Enlargement of the rectangular area shown in Fig. 1.

this cay is located on the northern side of the marginal line of the coral reef, rough waves incident from the Pacific Ocean break along the outer ridge of the coral reef, and waves attenuated by their breaking on the flat shallow reef are incident to the cay. In contrast, wind waves from the directions between the north and the east may occur, since this cay opens to Nakagusuku Bay in these directions.

Figure 3 shows a wind rose at Naha Airport 21 km distant from the cay in the WNW direction from Komaka Island. This wave rose was produced from the aeronautical climatological information given by the Japan Meteorological Agency (2021). The probability of wind direction in each specific range of 30 degrees was determined from the observation data between 2010 and 2014. The wind roses in a year can be classified into those formed in five periods: (1) January–March, (2) April and May, (3) June and July, (4) August and September, and (5) October–December. The typical wave rose in these periods is given as that observed in a specific month in each period.

In the first period, wind from the N30°E direction prevails, as typically shown by the wave rose in January. In the second period, wind blows from all the directions with no predominance, as given by the wave rose in April. In the third period, wind from the S30°W direction prevails, which is the reversed direction of that in winter. In the fourth period, there is no predominant wind direction, similarly to the second period, and in the fifth period, wind from the N30°E direction again prevails, similarly to that in the first period. In short, the predominant wind directions in winter and summer are N30°E and S30°W, respectively, in the vicinity of Komaka Island. Wind from the N30°E direction prevails, and there are no wave-sheltering islands that shorten the wind fetch along this direction; thus, wind waves can develop sufficiently in this direction. In contrast, wind waves from the S30°E direction are assumed to attenuate because of wide reefs on the south side of the cay.

Figure 4 shows an enlarged satellite image of the rectangular area shown in Fig. 2. At the north end of Komaka Island, a natural rock of 80 m width exists in the E–W direction, and a semicircular sandy beach is formed south of this rock, which is composed of coral debris and foraminifera remains. The coral reef well develops along the east side of the island compared with that on the west side, and a

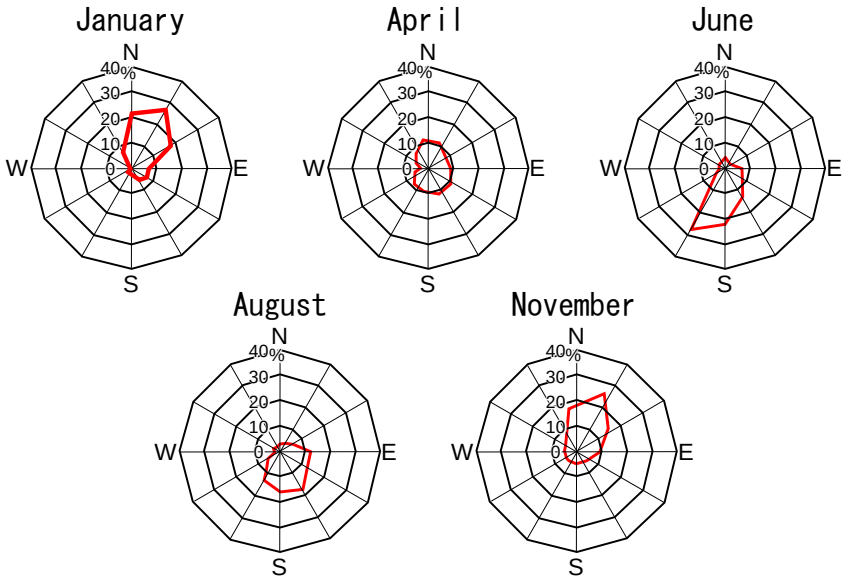

Figure 3. Wind rose at Naha Airport measured between 2010 and 2014.

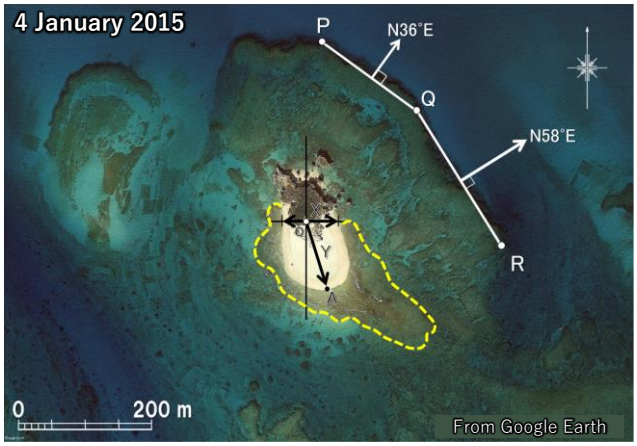

Figure 4. Satellite image of Komaka Island on 4 January 2015 and definition of coordinate system.

coral reef of 180 m width surrounds the island. The wind directions normal to the outer marginal line of the reef are N36°E and N58°E in the areas of PQ and QR, respectively, on the east side of the island, as shown in Fig. 4. The N36°E direction normal to the outer boundary, PQ, of the coral reef corresponds well to the predominant N30°E wind direction in winter, as shown in Fig. 3, implying that the coral reef extending along the eastern side of Komaka Island has mainly been formed owing to wind waves in winter.

Field observation of the shoreline changes on the cay under waves was carried out on 13 July 2019. The shoreline configuration was measured using satellite images and a GPS, and the variation in the planar configuration of the shoreline was determined from past satellite images. The present situation of the sandbar on the cay was observed at 17 points. The elevation of the sandbar above the mean sea level (MSL) was evaluated from tide levels at Naha Port at the same observation time. Then, the BG model was improved so that it can predict the planform changes in the shoreline configuration of the cay.

PLANFORM CHANGES IN SANDBAR ON KOMAKA ISLAND

The planform changes in the shoreline configuration of Komaka Island were investigated using eleven satellite images taken between 2009 and 2014. First, the origin O was fixed on a natural rock located at the center of the island (Fig. 4). Then, the beach width X was measured in the E–W direction from the origin to the east end of the beach. The distance between the origin and the location A at the furthermost distance from the origin on the south side was also measured as Y along with an aspect

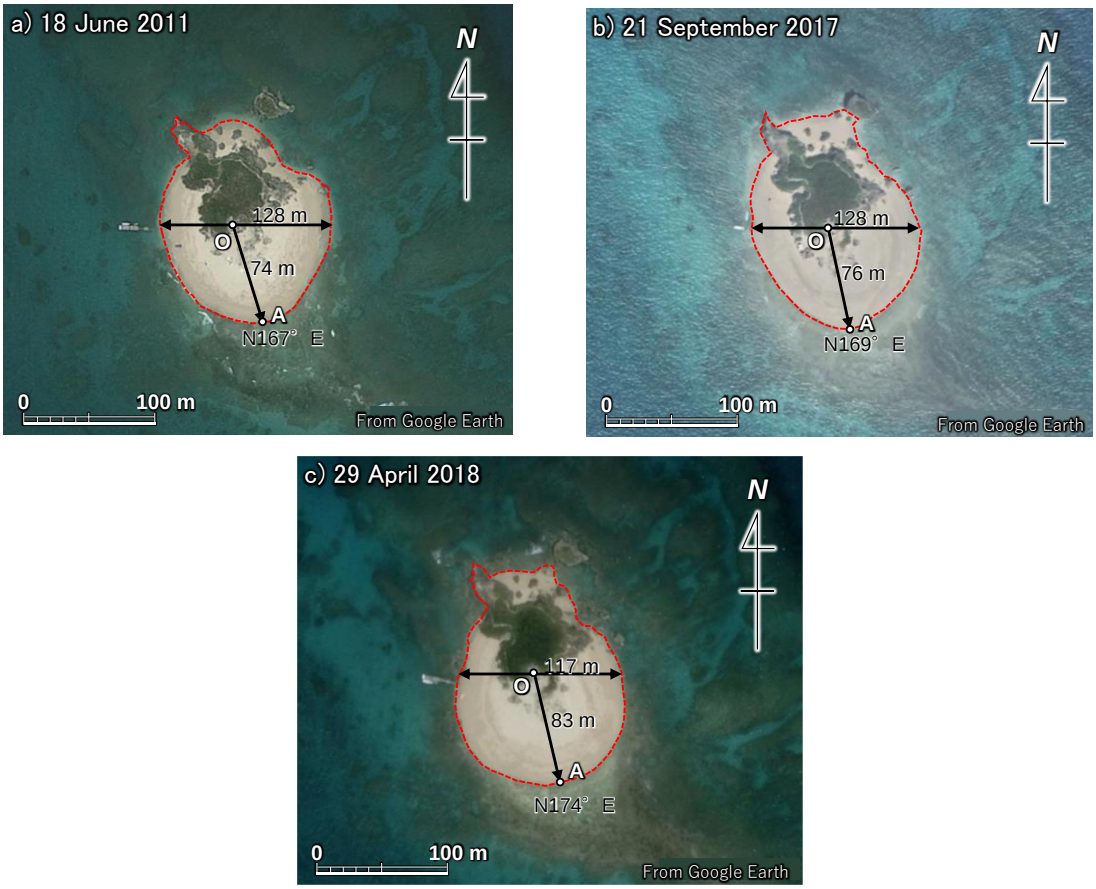

Figure 5. Satellite images of sandbar classified into Type I.

Table 1. Parameters of Types I, II, and III.

Type	Observation date	X (m)	Y (m)	Nθ°E	γ
I	18 June 2011	128	74	167	0.58
	21 September 2017	126	76	169	0.60
	29 April 2018	117	83	174	0.71
	Average	124	78	170	0.63
II	17 September 2009	88	109	174	1.25
	25 November 2012	88	94	168	1.08
	8 March 2013	95	95	171	0.99
	4 January 2015	83	106	169	1.28
	9 April 2018	85	98	163	1.15
	Average	88	100	169	1.15
III	19 January 2013	77	117	164	1.52
	17 October 2014	71	155	156	2.18
	20 November 2014	69	135	154	1.96
	Average	72	136	158	1.89

ratio of $\gamma = Y/X$. Moreover, the angle (θ) that OA makes with respect to the north was measured clockwise.

As a result of the classification of eleven satellite images, the shape of the sandbar was classified into one of three types: Types I (circular), II (slender oval), and III (elongated oval). Figure 5 shows a satellite image of the sandbar of Type I, and Table 1 summarizes the values of the parameters mentioned above. The mean sizes of the sandbar, such as X, OA, and γ were 124, 78 m, and 0.63.

Similarly, Fig. 6 shows the satellite images of the sandbar of Type II (oval shape) and Table 1 summarizes the characteristic scales of the sandbars. On average over five periods, X, OA, and γ were 88, 100 m, and 1.15, respectively. When comparing the shapes of the sandbar of Type II with those of Type I, X decreased by 29% from 124 m to 88 m in Type I, whereas OA increased by 28% from 78 m to 100 m, and γ increased by 83% from 0.63 to 1.15.

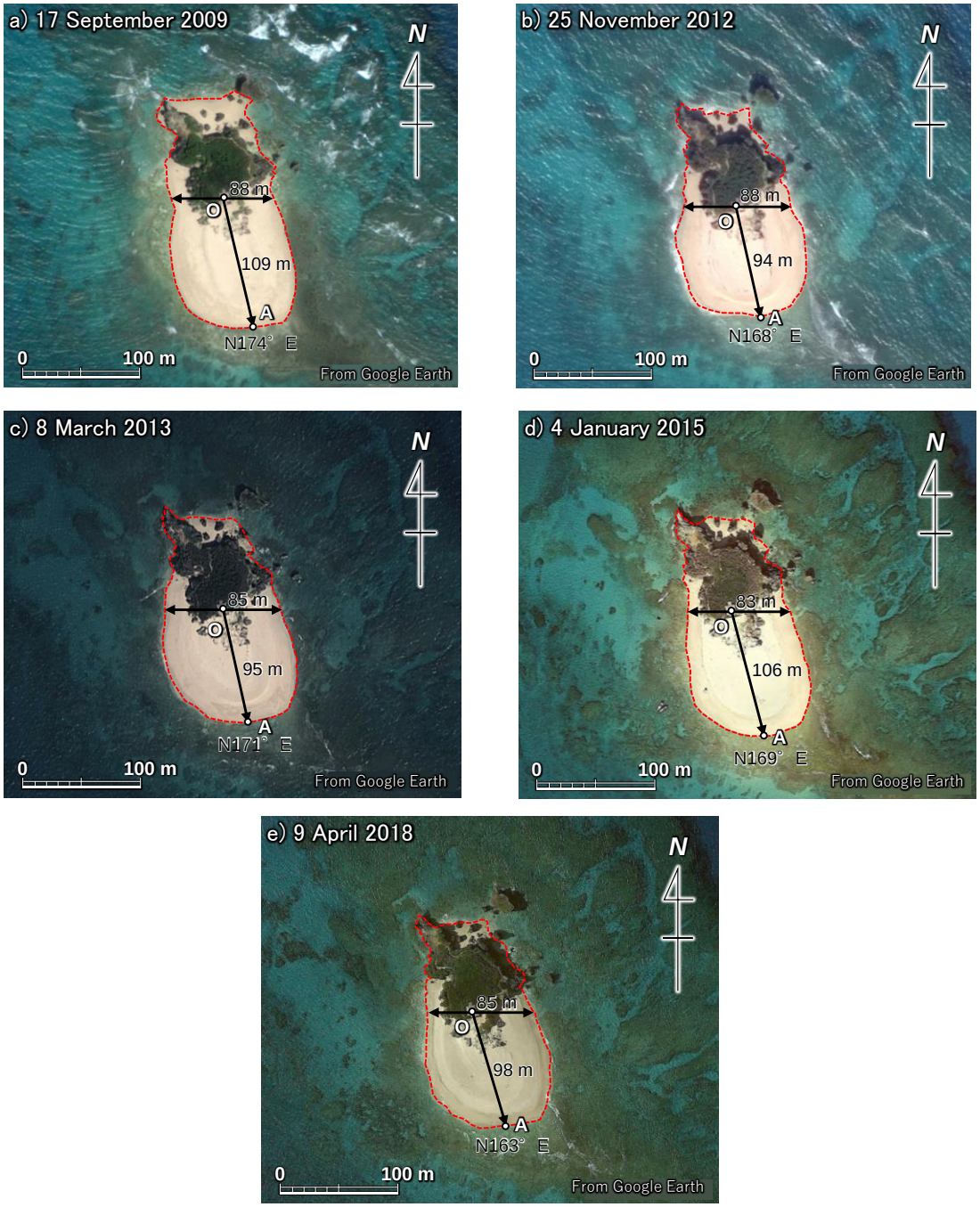

Figure 6. Satellite images of sandbar classified into Type II.

A Type III sandbar associated with the southward extension of a slender sandbar was measured three times, as shown in Fig. 7. In the case of the Type III, X, OA, and γ were 72, 136 m, and 1.89, respectively. In comparing with those in the Type I sandbar, X decreased by 42% from 124 to 72 m, whereas OA increased by 74% from 78 to 136 m, together with the increase in γ from 0.63 to 1.89, resulting in the southward elongation.

The foreshore area of the sandbar in each observation was calculated on the basis of the planform of the sandbars shown in Figs. 5–7, except for the rocky area located in the north part, and the temporal changes in the foreshore area and the ratio relative to the average area of the sandbar were calculated, as shown in Fig. 8. In the calculation, the change in shoreline position caused by the change in the tide level was not corrected, because the tide level when the satellite image was taken was not known. Therefore, some variations are included in the results. However, the foreshore area remained almost

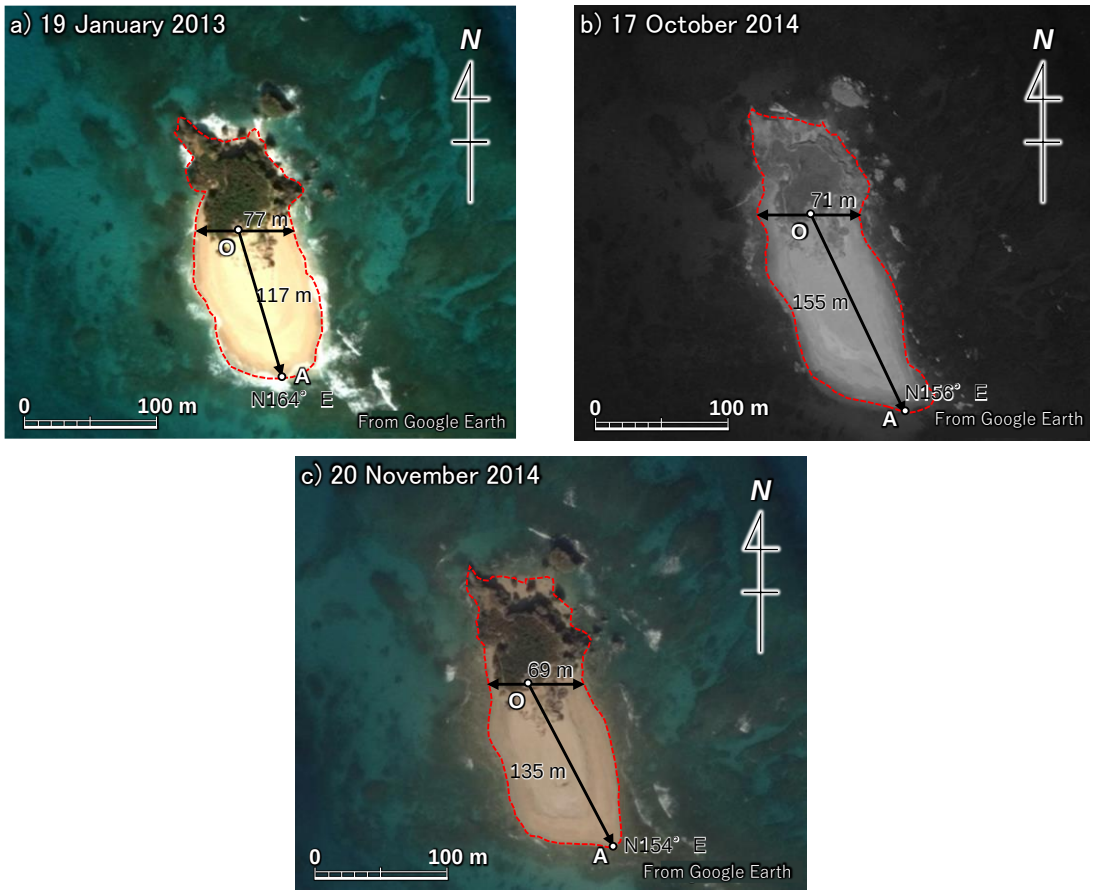

Figure 7. Satellite images of sandbar classified into Type III.

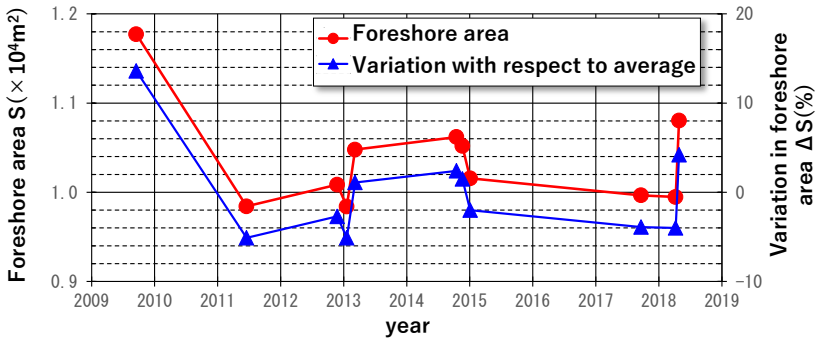

Figure 8. Temporal changes in planar area of sandbar and ratio of variation from mean value.

constant at 10,366 m^2, implying that the shape of the sandbar changes in response to changes in wave direction while satisfying the conservation of mass of sand.

The shape of Type I sandbar is approximately circular, so it is assumed that waves were incident to this cay with an equivalent probability of occurrence from all the directions around Komaka Island. Similarly, the Type II sandbar was subject to the action of wind waves from the N30°E direction, which is predominant in the winter months of October, November, and January, causing southward longshore sand transport, whereby the sandbar extends in the N169°E direction. Although the sandbar of Type III is also subject to waves in winter, similarly to that of Type II, a slender sandbar extended further in the N158°E direction because of the greater intensity of waves.

FIELD OBSERVATION OF SANDBAR OF CAY

In the field observation of the cay of Komaka Island, the shoreline configuration was measured using a GPS, and photographs were taken at 17 points around the cay. Figure 9 shows a satellite image of the cay taken on 29 April 2018 with the shoreline configuration measured on 13 July 2019

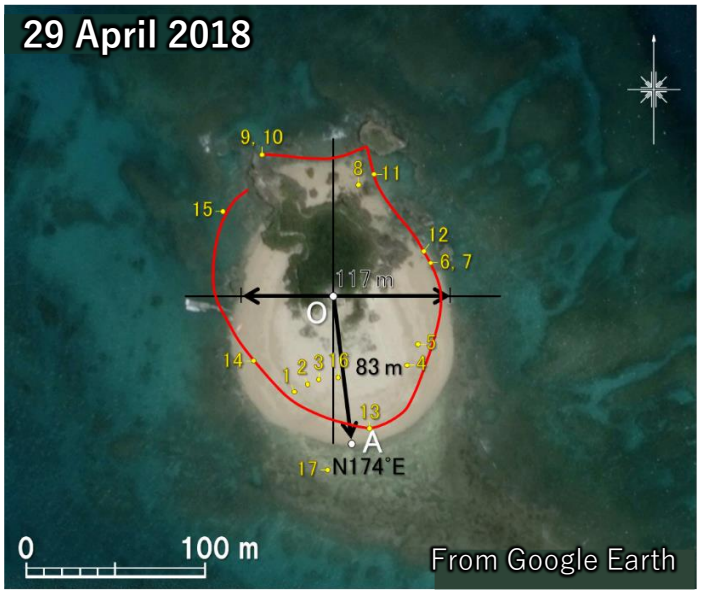

Figure 9. Satellite image of Komaka Island on 29 April 2018, shoreline configuration on 13 July 2019, and locations of Sts. 1–17 where photographs were taken.

concurrently with the locations of St. 1–17. Out of the 17 points, St. 2 was selected for the collection of foreshore material samples and the sieve analysis of the beach material was carried out. The shoreline configuration shown in Fig. 9 had the circular shape (i.e., Type I), because the shoreline was measured in the early summer. Sand deposited on the south side was transported northward under the waves incident from the south.

The characteristic results of field observation are shown in Fig. 10. First, Fig. 10(a) shows the shoreline condition on the southwest side of the cay, taken from St. 1. Sand was deposited on the exposed rocky coral bed, and the beach and the rocky bed of the flat reef were clearly separated by a line connecting the break in slope. The line smoothly connecting the locations of the break in slope slightly varies in the longshore direction because of the irregularity of the rocky bed, and the sandy beach and bedrock were approximately separated by a dotted line shown in Fig. 10(a). The tide level at Naha Port (above E.L.) measured by the Japan Meteorological Agency was E.L.−0.42 m at 9:35 on 13 July 2019 when the measurement was carried out. On the other hand, the elevation above sea level of the ground at St. 1 at 9:35 was +0.55 m; therefore, the elevation at St. 1 above E.L. of Naha Port became E.L. +0.13 m, where H.W.L. is given by E.L. +0.94 m.

At St. 2 located on the shoreface, as shown in Fig. 10(b), the foreshore slope was measured and beach material samples were collected. As a result, the foreshore slope was measured to be 1/9 and the beach material was well-sorted sand with a uniformity coefficient of 1.52, and the content of medium-size sand and d_{50} were 98.9% and 0.62 mm, respectively. Moreover, Fig. 10(c) shows the condition of the berm top at St. 3, and the upper beach was flat with the formation of a low scarp of 0.2 m height along the marginal line of the berm. The elevation of the flat surface landward of the berm, as shown in Fig. 10(c), was +1.93 m relative to the elevation at St. 1. In conclusion, it was found that on this coral cay, sand movement caused by waves occurs in a range between the break in slope separating the sandy beach and the flat bed of the reef and the berm height of approximately +1.93 m.

Figure 10(d) shows the condition of the point where the rocky bed connects with the sandy beach at St. 14 located on the west side of the cay, looking north. Here, again the sandy beach and the bedrock were clearly separated by a line connecting a break in slope. A sandy beach of a steep slope extended landward of a marginal line with a break in slope. A rock stands at the northwest end of the cay and fully blocked longshore sand transport (Fig.10(e)). Finally, Fig. 10(f) shows the condition of the sandy beach observed from St. 17 located at the south end of the cay. A flat rocky coral bed extends at the south side of the sandy beach, and sand was deposited on this flat rocky bed. The variation of the sandy beach occurs as a result of the movement of this sand. The upper surface of the sandy beach has a constant height, and the shape of the sandy beach changes while maintaining a constant elevation. In conclusion, it was found that a sandy beach with a foreshore slope of 1/9 was formed, and a flat sandy surface was formed with an elevation of 1.9 m above the position of the break in this slope.

Figure 10. Field conditions of six selected points (Sts. 1, 2, 3, 14, 15, and 17) on Komaka Island.

NUMERICAL SIMULATION OF DEFORMATION OF SANDBAR ON A CAY USING IMPROVED BG MODEL

In the model, a restoring force is assumed to be generated by the deviation in the shoreline configuration relative to the completely stable shoreline of a circular shape, similarly to the additional sand transport due to the distortion in the longshore distribution of the breaker height, as described by Ozasa and Brampton (1980). An additional sand transport is induced to compensate for this deviation, and the topography changes until two types of sand transport induced by the distortion of the shoreline and longshore distribution in wave height balance each other.

On Komaka Island, rough waves are mainly incident from the north in winter, causing the wave-sheltering effect of the island on its south side. Wave height decreases on the lee of the island, whereas it increases with distance from the island outside of the wave-shelter zone. Assuming a wave condition in which waves are predominantly incident from the north, the wave diffraction coefficient K_d can be assumed to have a radial distribution with respect to the center of the island with a large wave-sheltering effect on its south side, as schematically shown in Fig. 11. In the model, the change in K_d causes a spatial change in sand transport, because sand transport flux is expressed by the power 5/2 of the wave height.

The initial topography was assumed to be circular with a radius of 130 m, as shown in Fig. 12. The rock located at the center of the coral cay was given by a fixed boundary. The size of sand particles and the equilibrium slope were assumed to be 0.62 mm and 1/9 on the basis of the measured values, respectively. Waves with a significant wave height of 1 m were assumed to be incident on the coral cay. h_c and h_R were 3 and 1.5 m, respectively, and calculation was carried out up to 10^5 steps, given the time step of 0.1 h. The other calculation conditions are summarized in Table 2.

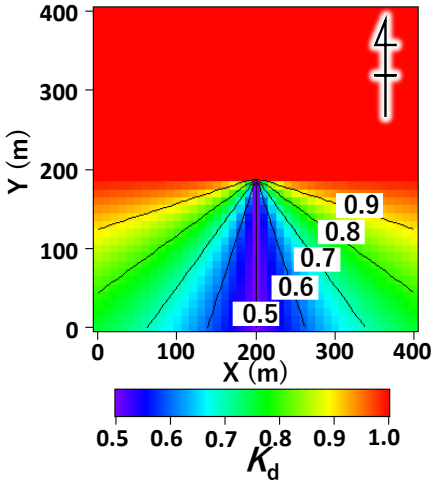

Figure 11. Distribution of K_d value employed in calculation.

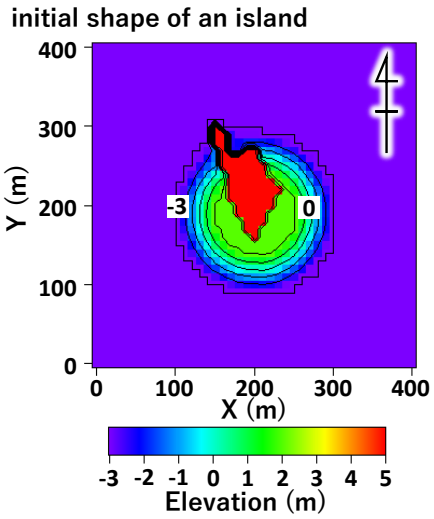

Figure 12. Initial shape of cay.

Table 2. Calculation conditions.

Grain size of sand, d	0.62 mm
Equilibrium slope	1/9
Tide level (M.S.L.)	0 m
Incident wave height, H	1.0 m
Berm height, h_R	2.06 m
Depth of closure, h_c	3.0 m
Depth distribution of sand transport	Uniform
Calculation domain in longshore and cross-shore directions	1000 m
Mesh size ($\Delta X = \Delta Y$)	10 m
Time step, Δt	0.1 h
Total time steps	10^5

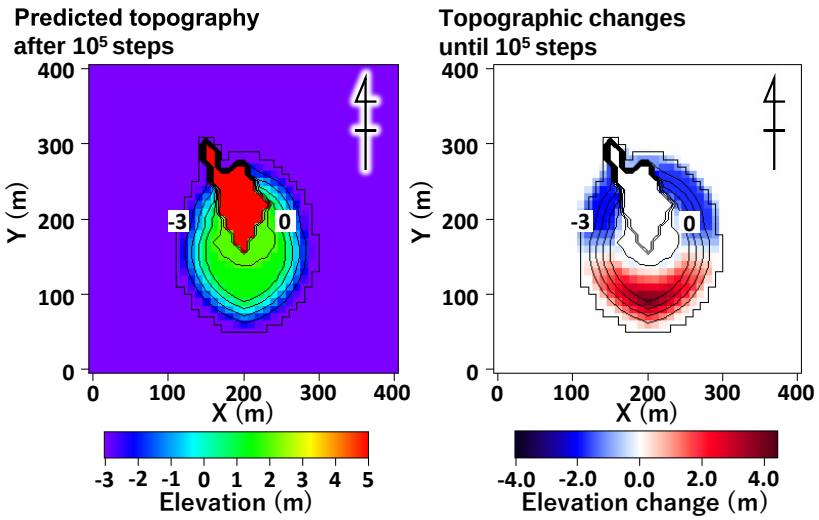

Figure 13. Predicted results of the cay and topographic changes after calculation of 10^5 steps.

Predicted results after 10^5 steps and the change in topography relative to the initial topography are shown in Figs. 13. The initial circular cay deformed owing to the action of waves incident from the north, resulting in erosion in the northern half of the island, and sand was transported to the lee of the cay. Thus, the shape of the cay became asymmetric. This result of the numerical simulation well explains the observed result of the deformation of the Type II sandbar on 4 January 2015 (Fig. 6(d)).

CONCLUSIONS

We adopted Komaka Island located 3 km offshore of Chinen Peninsula in Okinawa as the study site, and investigated the shoreline changes around a coral cay using satellite images. As a result, the shape of the sandbar behind the island was classified into one of three types (circular, slender oval, and elongated oval). Then, the BG model was improved in analogy with Ozasa and Brampton's theory, in which longshore sand transport is induced by the longshore inclination of the breaker height, given the distribution of K_d, and assuming that waves are incident from every direction so as to focus at the center of the circular island O. Under this condition, K_d was found to change owing to the wave-sheltering effect of the cay, and longshore sand transport is induced owing to the change in K_d in the direction normal to the wave direction. By calculation using the model, the deformation of the Type I sandbar, which is subject to strong wave action from the north, into Type II with southward elongation was qualitatively explained.

REFERENCES

Japan Meteorological Agency. 2021. https://www.jma-net.go.jp/naha-airport/tokusei/roah/windrose.html

Miyahara, S., Uda, T., and Serizawa, M. 2013. Prediction of topographic changes of a circular sandy island using BG model, *Asian and Pacific Coasts 2013*, Proc. 7th International Conf., 17–23.

Ozasa, H. and Brampton, A. H. 1980. Model for predicting the shoreline evolution of beaches backed by seawalls, *Coastal Eng.*, Vol. 4, 47–64.

Uda, T., Serizawa, M., and Miyahara, S. 2017. Seasonal movement of sand spits on a coral cay of Embudu Village Island in the Maldives, *Proc. 9th Int. Conf. on Asian and Pacific Coasts* (APAC2017), 467–478.

Serizawa, M., Uda, T., and Miyahara, S. 2014. Interaction between two circular sandy islands on flat shallow seabed owing to waves, *Proc. 34th ICCE*, 1–12. https://icce-ojs-tamu.tdl.org/icce/index.php/icce/article/view/7106/pdf_410

Uda, T., Serizawa, M., and Miyahara, S. 2018. Morphodynamic model for predicting beach changes based on Bagnold's concept and its applications, INTEC, London, UK, 188 pp. https://www.intechopen.com/books/morphodynamic-model-for-predicting-beach-changes-based-on-bagnold-s-concept-and-its-applications